Research Square

Preprints are preliminary reports that have not undergone peer review.
They should not be considered conclusive, used to inform clinical practice,
or referenced by the media as validated information.

Spatial scale of geomagnetic Pc5/Pi3 pulsations as a factor of their efficiency in generation of geomagnetically induced currents

Nadezda V. Yagova (nyagova@yandex.ru)
Schmidt Institute of Physics of the Earth https://orcid.org/0000-0003-0678-8743
Vyacheslav Pilipenko
Institut fiziki Zemli imeni O U Smidta Rossijskoj akademii nauk
Yaroslav Sakharov
Polarnyj geofiziceskij institut Rossijskaa akademia nauk
Vasily Selivanov
Kol'skij naucnyj centr Rossijskaa akademia nauk

Full paper

Keywords: geomagnetically-induced currents, Pc5/Pi3 geomagnetic pulsations

Posted Date: November 4th, 2020

DOI: https://doi.org/10.21203/rs.3.rs-39394/v2

License: This work is licensed under a Creative Commons Attribution 4.0 International License.
Read Full License

Version of Record: A version of this preprint was published at Earth, Planets and Space on April 14th, 2021. See the published version at https://doi.org/10.1186/s40623-021-01407-2.

Spatial scale of geomagnetic Pc5/Pi3 pulsations as a factor of their efficiency in generation of geomagnetically induced currents

Nadezda V Yagova[1,2*], Vyacheslav A Pilipenko[1,2], Yaroslav A Sakharov[3] and Vasily N Selivanov[4]

*Correspondence: nyagova@ifz.ru
[1]Schmidt Institute of Physics of the Earth of the Russian Academy of Sciences (IPE RAS), B. Gruzinskaya 10, Moscow, Russia
Full list of author information is available at the end of the article

Abstract

Geomagnetically induced currents (GICs) in a meridional power transmission line on the Kola Peninsula are analyzed during the intervals of Pc5/Pi3 (frequency range from 1.5 to 5 mHz) pulsations recorded at the IMAGE magnetometer network. We have analyzed GIC in a transformer at the terminal station Vykhodnoj (68° N, 33° E) during the entire year of 2015, near the maximum of 24-th Solar cycle. To quantify the efficiency of GIC generation by geomagnetic pulsations, a ratio between power spectral densities of GIC and magnetic field variations is introduced. Upon examination of the geomagnetic pulsation efficiency in GIC generation, the emphasis is given to its dependence on frequency and spatial scale. To estimate pulsation spatial scales in latitudinal and longitudinal directions, the triangle of stations KEV-SOD-KIL has been used. Large-scale pulsations (with a high spectral coherence, low phase difference, and similar amplitudes at latitudinally separated stations) are found to be more effective in GIC generation than small-scale pulsations. The GIC response also depends on the pulsation scale across the electric power line.

Keywords: geomagnetically-induced currents; Pc5/Pi3 geomagnetic pulsations

Introduction

Interaction of solar ejecta with the near-Earth environment activate global space weather processes: intensification of the magnetosphere - ionosphere current systems, energization of ring current and radiation belt particles, enhanced precipitation into the auroral oval, disturbance of the geomagnetic field, etc. These processes are potentially risky for space and ground technologies. Generation of geomagnetically induced currents (GICs) related to abrupt changes of the geomagnetic field is one of the most significant space weather factors for power transmission lines (e.g., Boteler (2001); Kappenman (2004)). Therefore, the geophysical community is making tremendous efforts to elaborate a global computer model of storm/substorm activity augmented by the magnetotelluric reconstruction of telluric currents (Love et al, 2018; Pulkkinen, 2015; Pulkkinen et al, 2007).

However, high-risk GICs may be related not only to global processes with an enormous energy yield (e.g., for typical substorm it is of 10^{14} J), but also to more localized and rapid processes. The solar wind-magnetosphere interaction results in the occurrence of diverse types of perturbations with various spatial and time scales. Such localized and fast disturbances embedded into the global magnetospheric processes may be the actual drivers of GIC bursts (Belakhovsky et al, 2019). In general,

the amplitudes of geomagnetic variations decrease with frequency, whereas the induced electric field magnitudes are expected to grow with frequency. Therefore, the GIC response, which is a convolution of both factors, must have a maximum at some frequencies. Many case studies of GIC bursts demonstrated that this time scale is about 2-10 min. That is, it falls into the band of Pc5/Pi3 pulsations, i.e. at the low-frequency edge of the ultra-low frequency (ULF) range.

The impulsive geomagnetic disturbances during nighttime may be associated with substorm onsets and subsequent activations, magnetic perturbation events - isolated disturbance with the duration of about 5-10 minutes (Engebretson et al, 2019), intense Ps6/Pi3 pulsations - quasi-periodic series of impulses with duration 10-20 min, and narrow band Pc5 pulsations with frequencies ∼2-7 mHz. Though the power of such processes is much lower than the power of magnetospheric storms and substorms, the rapidly varying electromagnetic fields of these disturbances can induce a significant GIC (Apatenkov et al, 2004; Belakhovsky et al, 2018; Viljanen, 1998). The events were presented when the ULF variations of the Pi3 or Ps6 type induced GIC in power transmission line up to 120 A (Apatenkov et al, 2020; Belakhovsky et al, 2019).

Viljanen et al (2001) suggested that the Pc5 waves during the recovery phase of a magnetic storm may cause intense GICs. Pulkkinen and Kataoka (2006) further proposed that a moderate and steady wave activity could lead to cumulative GIC effects such as corrosion of natural gas pipelines. Especially global Pc5 waves - anomalously intense pulsations at the recovery phase of strong magnetic storms, could be very effective GIC drivers (Marin et al, 2014). The actual driver of GICs - telluric electric field, can be estimated for a given magnetic field $B(f)$ varying with the frequency f above a homogeneous ground with the conductivity σ from the boundary impedance condition (in the plane wave approximation) as $E/B = \omega^{1/2}(\mu\sigma)^{-1/2}$, where $\omega = 2\pi f$, and mu is the magnetic constant. For the Pc5 pulsations with $\omega = 0.01$ s^{-1} and the average conductivity in Fennoscandia $\sigma = 10^{-4}$ S/m this relation gives E[mV/km]/B[nT]≈ 12 (mV/km)/nT. For the global Pc5 pulsations with $B \approx 100$ nT, the expected telluric field can reach $E \approx 10^3$ mV/km. This value is almost as high as the estimate given by Lucas et al (2020) for the extreme once-per-century electro-telluric field over the US territory.

Geomagnetic pulsations on the ground are the image of magnetohydrodynamic (MHD) waves in the magnetosphere. The ULF wave activity is controlled by the solar wind-magnetosphere interaction and processes inside the magnetosphere. The common view is that pulsations of extra-magnetospheric origin have longer azimuthal wavelengths than pulsations generated via wave-particle interaction inside the magnetosphere (Baker et al, 2003; James et al, 2013). Small-scale pulsations at auroral latitudes are the result of different kinetic processes (see, e.g. Baddeley et al (2004); Mager et al (2013)). These waves are severely screened by the ionosphere, and are almost undetectable on the ground surface.

The terrestrial magnetosphere forms a wide variety of MHD resonators and waveguides for ULF waves resulting in an essentially inhomogeneous ULF wave electromagnetic field. Additionally, the occurrence of strong gradients of the ionospheric conductivity and the ground geoelectric parameters may cause a non-uniform geomagnetic response even to large-scale magnetospheric sources (e.g. Alperovich and

Fedorov (2007); Mazur and Chuiko (2017)). Indeed, telluric electric field in realistic conditions is found to be more inhomogeneous in amplitude and direction than the primary magnetic field variations because of horizontal inhomogeneity of crust electric conductivity. Bedrosian and Love (2015) demonstrated that a telluric E-field can exhibit rapid spatial variations even in the presence of a spatially uniform B-field.

These factors lead to an essential difference between the spatial structures of geomagnetic pulsations and global processes like storms and substorms. In most cases, plane wave approximation provides good agreement between modeled and measured GICs during global storm-time disturbances (Viljanen et al, 2004). On the contrary, spatial distribution of pulsation magnetic field is essentially non-uniform even for narrow-band Pc pulsations. These effects are studied in details for the vicinity of Alfven Filed line resonance (FLR) latitude (Menk et al, 2004; Pilipenko et al, 1999; Sandhu et al, 2018), plasmapause projection (Kale et al, 2007; Milling et al, 2001) and equatorial electrojet (Fedorov et al, 1999).

In almost all previous studies of the relationship between GIC and geomagnetic variations, it was implicitly assumed that the magnetic field is homogeneous along an electric power line (EPL). The role of a geomagnetic variation spatial scale has never been thoroughly examined, although the importance of this effect has been postulated (e.g. Boteler and Pirjola (2017); Yagova et al (2018)).

Recently, a correlation between GIC and geomagnetic spectral amplitudes depending on pulsation spatial scale was studied by Sakharov et al (2021). Probability density function (PDF) of correlation between the spectral amplitudes of GIC and geomagnetic variations was calculated for the conductivity distributions corresponding to GIC J to B_Y spectral amplitude ratio with a power-law dependence on frequency

$$J \propto f^{\alpha} B_Y. \qquad (1)$$

This class of functions at $\alpha = 1$ and 0.5 describes two important models of electric conductivity distribution with depth. $\alpha = 1$ corresponds to GIC proportional to $\mathrm{d}B/\mathrm{d}t$. Such dependence relates to the "electrotechnical" model, when EMF is generated in circuit formed by the EPL and a thin conductive layer at a fixed depth. The model of constant Earth conductivity results in $\alpha = 0.5$ in Eq.(1). It was shown that the correlation between GIC and geomagnetic amplitudes is essentially higher for the large-scale pulsations than for small-scale ones. Meanwhile, no essential difference was found for conductivity models with $\alpha = 0.5$ and 1 in the Eq.(1). This result prompts that ULF pulsation spatial scale may be an important though underestimated factor in GIC generation. Here, we consider in detail the GIC dependence on pulsation spatial scale.

Data Set and Event Analysis Technique

The data of the IMAGE magnetometer network (10-sec cadence) (Tanskanen, 2009) are used for the analysis of geomagnetic field variations. The GIC recordings are provided by the system deployed in the "Northern Transit" EPL at the Kola Peninsula by the Polar Geophysical Institute and the Center for Northern Energetics (Viljanen

et al, 2012). This 330 kV power line is oriented along the magnetic meridian. We use the data from the terminal station Vykhodnoi (VKH) located at the corrected geomagnetic (CGM) latitude $\Phi = 65°$. The station records a quasi-DC current in the dead-grounded neutral of a transformer with a 1-min sampling rate. We analyze the Pc5/Pi3s pulsations detected during the year of 2015.

Kevo (KEV) magnetic station, the nearest to VKH and nearly at the same geomagnetic latitude, is taken as the basic one. Sodankylä (SOD) and Kilpisjärvi (KIL) stations are used for estimates of the pulsation's meridional and latitudinal spatial scales, respectively. Station locations are shown on the map (Figure 1) and the station information is summarized in Table 1.

The following data analysis technique has been used. Geomagnetic data is filtered in a $0.8-8.3$ mHz band and then decimated to a 1-minute sampling rate. GIC data is high-pass filtered with the 0.8 mHz cutoff frequency. Then, the spectral estimates are made in a 64 point (3840 s) running window with a 5-min shift between subsequent intervals. The power spectral density (PSD) is calculated with the Blackmann-Tukey method (Kay, 1988). Spectral coherence γ^2 and phase difference $\Delta\varphi$ are obtained from cross spectra. Periodic ULF disturbances are automatically selected with a detection program for the time intervals with a pronounced spectral maximum over the background "colored noise" spectrum (Yagova et al, 2015). The results of this selection have been visually checked. The bandwidth analyzed comprises the Pi3 range (predominantly $f < 2$ mHz) and Pc5 range ($f > 1.7$ mHz).

Efficiency of GIC generation is taken into account with the $R_{I-B}(f)$ parameter, which is the ratio of PSDs of GIC variations and geomagnetic pulsations at a given frequency. This ratio is calculated for each Pc5/Pi3 interval. Then, the R_{I-B} dependence on frequency and parameters characterizing spatial structure of geomagnetic pulsations is analyzed statistically. The variability of horizontal components of geomagnetic field $d\mathbf{B}/dt$ was found to be more isotropic than magnetic field disturbance $\Delta\mathbf{B}$ (Bedrosian and Love, 2015). However, the previous study of (Sakharov et al, 2021) has shown that for the latitudinally extended "Northern Transit" EPL correlation of GIC with B_Y component is higher, than that for the B_X component. Therefore, here the influence on GIC generation of B_Y component only is examined.

Both the absolute values and angles between the wave amplitude and phase gradients and the EPL are important for GIC generation. First, we examine how does the efficiency of GIC generation by Pc5/Pi3 pulsations depend on the pulsation's scale across the EPL. For that, we analyze the East-West (E-W) structure of pulsation magnetic field. Auroral Pc5 pulsations are typically large-scale in azimuthal direction, so their amplitudes and spectral content are almost constant along geomagnetic parallel at distances up to several hundred kilometers (Baker et al, 2003; Chisham and Mann, 1999). For such pulsations, even a mismatch of about few hundred kilometers in longitude between the magnetometer location and EPL is not significant. However, at auroral latitudes ULF pulsations with essential variation of amplitude and phase along geomagnetic longitude are also possible (Chisham and Mann, 1999). Yagova et al (2018) presented examples of Pi3 pulsations localized in the E-W direction and prolongated in the N-S direction. In this situation, magnetic pulsations at an EPL longitude can differ essentially from pulsations at the longitude of a magnetic station. For such E-W short-scale pulsations, any estimates of

GIC amplitude in an EPL would be inaccurate, if the magnetic data is taken from a station located far from the EPL meridian. That is why, spatial distribution of pulsation magnetic field in the E-W direction is to be taken into account for GIC applications.

For the further analysis, we use the same classification of the large- and small-scale pulsations, as in (Sakharov et al, 2021). For the classification of pulsations into E-W large- and small-scale, we use the KEV-KIL station pair. KIL is separated from KEV by $\Delta\Lambda = 5.5°$ (250 km). Amplitude variation is taken into account with the East-to-West (KEV/KIL) PSD ratio $R_{EW,By}$.

We define a Pc5/Pi3 pulsation as E-W large-scale, if $R_{EW,By}$ is close to 1 and spectral coherence γ^2_{EW} is high. The notation L_{EW} is used for these pulsations All the other pulsations are considered as short-scale in the E-W direction and referred to as S_{EW}.

A hypothesis to check is that the L_{EW} pulsations demonstrate higher spectral coherence with GIC variations than the S_{EW} ones.

As for the pulsation scale parallel to an EPL, it influences GIC amplitude, if the amplitude and/or phase of the pulsation changes essentially at the power line length. GIC to magnetic field PSD ratio is controlled by the shorter between the EPL length and pulsation's scale. Amplitude and phase distributions of real pulsation field are not identical to those of a plane wave. Thus, the pulsation spatial scales, obtained from amplitude and phase spatial distributions, can be different. Phase difference is of critical importance for GIC efficiency, because only in the case of small phase difference at EPL length, time derivative of the magnetic field $\mathrm{d}B/\mathrm{d}t$ has the same polarity throughout the EPL. Amplitude distribution along the meridian is the second factor, which also influences GIC amplitude. For nearly in-phase pulsations, GIC amplitude is determined by the amplitude averaged over EPL length.

In our consideration, we use the data from the KEV-SOD station pair for the analysis of Pc5/Pi3 magnetic field distribution along the meridian. SOD is located at $\Phi = 67.37°$, i.e. it is shifted by $\Delta\Phi = 2.4°$ (270 km) to the South from KEV. The magnetic latitudes of these two stations correspond to the Northern part of the EPL latitudes. In such a geometry, the pulsation efficiency should be higher for pulsations with higher South-to-North PSD ratio $R_{SN,By}$. That is, we define a pulsation as N-S large-scale (L_{NS}), if high spectral coherence, low phase difference, and high South-to-North PSD ratio are found at KEV-KIL station pair.

A hypothesis to check is that L_{NS} pulsations generate more intensive GICs than S_{NS} ones of the same amplitude and frequency, i.e. that the R_{I-By} is higher for the L_{NS} than for the S_{NS} pulsations.

The boundary values for coherence, phase difference and South-to-North PSD ratio are equal to $\gamma_b = 0.7$, $\mu_b = 0.85$ ($\mu = cos(\Delta\varphi)$), and $R_{SN,By} = 0.5$, respectively. These values provide comparable number of events in each of pulsation sub-groups.

Results

Examples of Pc5s with different GIC efficiency

A large-scale pulsation registered on 1 March 2015 (day 60) at 7:15 UT

Waveforms and spectral parameters of Pc5 pulsations recorded simultaneously in geomagnetic field at KEV and in GIC at VKH are given in Figure 2. The pulsation's main period is approximately 4 minutes. The peak-to-peak amplitude of the

pulsation varies from 20 to 40 nT for the geomagnetic field and from 5 to 10 A for the GIC (Figure 2a). Both magnetic field components and GIC PSD spectra demonstrate maxima at $f_1 = 1.7$, $f_2 = 2.7$, and $f_3 = 4$ mHz (Figure 2b). Spectral coherence γ^2_{I-By} (Figure 2c) is almost 1 at all the frequency band $1.7-5$ mHz. This panel also shows spectral coherence γ^2_{I-Bx} between the B_X component and GIC. Although it exceeds 0.5, it is lower than γ^2_{I-By} at all the frequencies analyzed. GIC to B_Y PSD ratio R_{I-By} varies in the range of $0.01 - 0.03$ A^2/nT^2 and it has a maximum at the f_2 frequency and it grows with frequency at $f > 3.3$ mHz (Figure 2d).

What about the spatial properties of this pulsation? Distribution of the pulsation parameters along the latitude are illustrated by Figure 3. For the KEV-KIL station pair, the pulsation's waveforms are similar (Figure 3a). This is also confirmed by spectral parameters (Figure 3, b-d). The spectral coherence $\gamma^2_{EW,By}$ exceeds 0.5 (Figure 3c) at frequencies of all the spectral maxima found in KEV PSD spectrum. As for B_X component, $\gamma^2_{EW,Bx}$ is almost 1.

Figure 3d depicts East-to-West PSD spectral ratio for both horizontal components. $R_{EW,By}$ at these frequencies exceeds 1. This means that spectral power grows at this longitude interval towards noon and is higher at KEV than at KIL. $R_{EW,Bx}$ is even higher, than $R_{EW,By}$, and it exceeds 1 at all the analyzed frequencies.

Thus, we classify this as an E-W large-scale pulsation. Found spectral ratio and coherence allow us to suggest that at the EPL longitude, the pulsation should have nearly the same spectral content, as at KEV, and a comparable (or, probably, somewhat higher) amplitude.

Distribution of the pulsation parameters along the meridian are illustrated by Figure 4. Waveforms for both horizontal components are shown on the left of the Figure (4a,b). The B_Y pulsation is clearly seen at SOD, but its amplitude is lower, than at KEV. Spectral coherence is almost 1 for all the spectral maxima. At f_1 frequency, pulsations are in phase. At two higher frequencies, phase difference does not exceed 25°. Thus, dB_Y/dt polarity remains the same during almost all of the pulsation half-period. The South-to-North PSD ratio changes from 1 at 1.7 mHz to about 0.3 at the frequencies of two other spectral maxima (note, that 0.3 in PSD spectral ratio corresponds to 0.55 in amplitude spectral ratio). The variations of B_X component are almost counter-phased to B_Y. Meanwhile, spectral content differs between the components. Thus, PSD of B_X has the main maximum at f_2, and it is higher than that of B_Y. The absolute value of phase difference in B_X does not exceed 45° at $f < 4$ mHz, and its sign at f_2 is positive, in contrast to that in B_Y. The South-to-North PSD ratio in B_X is about 0.3 at these frequencies.

At frequencies below 4 mHz, the pulsation is polarized almost linearly. However, the difference between the two components is seen in the PSD and phase spectra near f_2. This can result from FLR at L-shell somewhere between KEV and SOD. Actually, near f_2, B_X component demonstrates all the typical resonance features, i.e. clear PSD maximum (Figure 4c), apparent propagation from South to North (Figure 4b,e), and extended South to North PSD ratio (Baransky et al, 1995).

We can summarize, that this pulsation demonstrates high coherence and low phase difference in both horizontal components. Thus, we classify this as a large-scale pulsation in the N-S direction. We expect that it should be effective for GIC generation.

Actually, GIC to B_Y PSD ratio varies with frequency in the $0.01 - 0.03$ A^2/nT^2 range (i.e., $0.1 - 0.2$ A/nT in the amplitude spectra).

A small-scale pulsation registered on 12 May 2015 (day 132) at 4:05 UT

A pulsation recorded in the early morning (7 MLT at KEV) of May 12 is illustrated in Figure 5. Peak-to-peak amplitude of the geomagnetic pulsation at KEV reaches 60 nT. Simultaneously, the pulsation is seen in GIC with amplitude of about 1 A (Figure 5a). A main spectral maximum is found in the PSD spectra at $f_1 = 2.1$ mHz, and a minor maximum - at $f_2 = 3.7$ mHz (Figure 5b). Both frequencies are stressed in coherence spectrum, as well. Coherence between GIC and B_X is lower than that between GIC and B_Y (Figure 5c). It should also be noted, that spectral coherence is lower than in the previous event. The GIC to B_Y PSD ratio varies near $R_{I-By} = 3 \cdot 10^{-4}$ A^2/nT^2 (Figure 5d), i.e. it is two orders of magnitude lower, than for the previous event.

Pulsation waveforms for the KEV-KIL station pair and their spectral parameters are presented in Figure 6. The B_Y pulsation is seen at both stations with similar waveforms and comparable amplitudes (Figure 6a). Both frequencies of spectral maxima at KEV, can also be seen in KIL PSD spectrum (Figure 6b). However, a maximum in coherence spectrum is only found for f_1 frequency with $\gamma^2 = 0.9$, while at f_2, γ^2 is about 0.5. The B_X coherence spectrum is similar to that of B_Y at $f < 2.4$ mHz and then $\gamma^2_{EW,Bx}$ decreases with f quicker than $\gamma^2_{EW,By}$. For the B_X component, the East-to-West PSD ratio $R_{EW,Bx}$ exceeds 1 at all frequencies, while for B_Y, it is nearly 1 at f_1 and about 0.3 at f_2. This allows us to assume that the pulsation should be seen in B_Y at the VKH longitude with an amplitude close to that at KEV at f_1 and with a somewhat lower amplitude at f_2.

Distribution of the pulsation parameters along the meridian are shown in Figure 7. In both components, the pulsation is seen at the KEV and SOD stations with similar apparent periods, but its amplitude and phase differ essentially (note, that we use a different vertical scale for two stations to make the pulsation at SOD visible). As a result, dB_Y/dt polarity remains the same between KEV and SOD only during approximately a fourth of the pulsation period (is only half compared to the previous case). The spectral peak at f_1 frequency is seen in both the PSD and coherence spectra (Figure 7, cd). As for the South-to-North PSD ratio, it is about 0.03 (0.2 in the amplitude spectra). B_X coherence is lower, phase difference is nearly the same, and $R_{SN,Bx}$ is higher than the corresponding parameters for B_Y component.

According to the selection criteria, this pulsation is small-scale in both directions. A comparison of pulsation amplitudes in GIC and geomagnetic components for the two events analyzed demonstrates that the first pulsation is more effective in GIC generation than the second one. In fact, the GIC amplitude during the second interval is only about 1 A, i.e. it is an order of magnitude lower than for the first event, while the amplitude of the geomagnetic pulsation is higher in the second case. We assume that this results from the difference of spatial scales of the pulsations. In the next subsection we shall verify this assumption using the analysis of pulsations registered in B_Y component of the geomagnetic field and GIC during the year 2015.

Statistics

Pulsation scale in the E-W direction (i.e. transversal to the EPL) influences GIC parameters due to the fact that magnetic stations are usually not co-located with an EPL. Thus, the magnetic data used for GIC estimates is not exactly the same, as at the EPL longitude. When magnetic field is recorded not at an EPL longitude and the acquired data is utilized to estimate GIC parameters in the EPL, some kind of interpolation procedure is explicitly or implicitly used. This can lead to essential or negligible errors depending on E-W inhomogeneity of pulsation magnetic field.

Spectral coherence γ^2_{I-By} quantifies the inter-dependence between GIC and magnetic field variations. Figure 8 shows empirical PDFs, calculated as $F = n_i/N_t$, where n_i is the number of Pc5/Pi3 intervals with $\gamma^2_{I-By} \in \Delta\gamma^2_i$, $\Delta\gamma^2_i = (\gamma^2_i, \gamma^2_{i+1})$ and $N_t = \sum(n_i \Delta\gamma^2_i)$. In the Figure, the distributions of Pc5/Pi3 intervals over γ^2_{I-By} are given separately for the L_{EW} and S_{EW} pulsations. The difference in distributions is clearly seen in all the frequency bands. A fraction of low-coherent intervals is essentially higher for small-scale pulsations, while the large-scale pulsations demonstrate a pronounced high-coherence maxima at all frequencies.

The efficiency of Pc5/Pi3s in GIC generation depends on their spatial scale in the N-S direction. N-S large-scale pulsations generate GICs with the amplitudes higher, than N-S small-scale pulsations of the same amplitude. This effect is seen in the GIC to B_Y PSD ratio R_{I-By}. Figure 9 shows R_{I-By} normalized PDFs for (L_{NS}) and small-scale (S_{NS}) pulsations. For all the frequency bands, the distributions for small-scale pulsations are enriched with low values of R_{I-By}. At the two lower frequencies, the most probable value of R_{I-By} is the same for the two groups of pulsations, while for the two higher frequencies, the most probable R_{I-By} is also higher for the large-scale pulsations. The fraction of $R_{I-By} > 0.1$ A^2/nT^2 (0.3 A/nT in amplitude spectra) is nearly two times higher for the large-scale pulsations, than for the small-scale ones in all the frequency bands. As for the rare events ($F^* \simeq 10^{-3}$) with extremely high values of $R_{I-By} \geq 1$ A^2/nT^2, their fraction is even higher for the small-scale pulsations, than for the large-scale ones. This effect should be a point of a special study.

Actually, we have used three parameters to discriminate between large-scale and small-scale pulsations, namely, the spectral coherence, phase difference, and South-to-North PSD ratio. In a real wave, they are not independent. However, we can try to discriminate between their influence on R_{I-By}. A low coherence at a given frequency means that the phase difference changes essentially during the time interval, for which the spectrum is calculated. Thus, phase difference estimates are valid only for coherent pulsations. We expect that the coherence and phase difference influence R_{I-By} in a similar way, because both the low coherence and high phase difference at the EPL length lead to a situation, where different EPL segments contribute to EMF with the opposite signs. On the contrary, the South-to-North PSD ratio $R_{SN,By}$, influences the GIC only via EMF amplitude variation along the EPL. Thus, the R_{I-By} dependence on the $R_{SN,By}$ is expected to be weaker than its dependence on coherence and phase difference.

Figure 10 illustrates pulsation efficiency in GIC generation depending on their coherence, phase, and PSD distribution along the magnetic meridian. For that, R_{I-By} spectra averaged over each of the emerging 6 groups of pulsations are calculated.

First, we divide pulsations into small- and large-scale ones, depending on their spectral coherence (marked S_γ and L_γ in the Figure). This first division allows us to analyze phase distribution for the group of coherent pulsations (L_γ). The L_γ group is divided into small- and large-scale sub-groups in accordance to their phase difference ($L_\gamma S_\varphi$ and $L_\gamma L_\varphi$ in the Figure). At the last stage, we divide the $L_\gamma L_\varphi$ group into small- and large-scale sub-groups depending on their South-to-North PSD ratio $R_{SN,By}$ ($L_\gamma L_\varphi S_P$ and $L_\gamma L_\varphi L_P$ in the Figure).

The average value of R_{I-By} ratio is nearly 3 times higher for the L_γ and $L_\gamma L_\varphi$ groups than for the S_γ and $L_\gamma S_\varphi$ ones. This means that low coherence and high phase difference lead to a comparable decrease of pulsation efficiency in GIC generation.

R_{I-By} for one group of pulsations demonstrates specific spectral features at the high frequency flank of the frequency band analyzed, i.e. in the vicinity of Alfven resonance frequency at KEV. In contrast to the other groups, R_{I-By} frequency dependence is not monotonous for the $L_\gamma S_\varphi$ group. It has a maximum at $f =$ 3.3 mHz and its value at this frequency is approximately two times higher, than at the frequency of a local minimum at $f = 3.7$ mHz. This effect should be taken into account in estimates of expected GIC amplitudes.

A dependence of pulsation efficiency in GIC generation on amplitude distribution of pulsation's magnetic field can be seen from the comparison of R_{I-By} spectra of the $L_\gamma L_\varphi L_P$ and $L_\gamma L_\varphi S_P$ groups. One can see from the Figure, that R_{I-By} for the pulsations defined as large-scale with all three parameters ($L_\gamma L_\varphi L_P$ group) is about 2 times higher than that for the $L_\gamma L_\varphi S_P$ group. This demonstrates that the PSD meridional distribution has a weaker influence on the efficiency of GIC generation than phase distribution. As for the R_{I-By} ratio for the most effective $L_\gamma L_\varphi L_P$ group, it is 4 times higher than that for the S_γ group, for which the GIC efficiency is minimal. This corresponds to a two times higher GIC amplitude for the same amplitude of geomagnetic pulsations.

In the final analysis, we return to the classification of pulsations into two groups and define only the $L_\gamma L_\varphi L_P$ group, as large-scale (L_{NS}). All the other pulsations are considered to be small-scale (S_{NS}). The resulting averaged R_{I-By} spectra for these two groups are given in Figure 11(a). The large-scale pulsations produce a higher average PSD in GIC than the small-scale ones. The R_{I-By} ratio grows from $1.5 \cdot 10^{-2}$ $\mathrm{A^2/nT^2}$ at 1.5 mHz to $4.4 \cdot 10^{-2}$ $\mathrm{A^2/nT^2}$ at 5 mHz for the large-scale pulsations and from $5 \cdot 10^{-3}$ to $2.2 \cdot 10^{-2}$ $\mathrm{A^2/nT^2}$ for the small-scale ones. Its value averaged over the frequency band is three times higher for the large-scale pulsations than for the small-scale ones.

The slopes of the R_{I-By} spectra differ for the two groups of pulsations. For the large-scale pulsations, it corresponds to a model of constant crust conductivity ($\alpha = 0.5$ in the Eq.(1)). The spectrum for the S_{NS} pulsations is close to linear dependence of GIC amplitude on frequency. This means that the electric current is roughly proportional to $\mathrm{d}B_Y/\mathrm{d}t$.

The pulsations' efficiency in GIC production is characterized not only by the mean values of GIC amplitudes, but also by a fraction of high R_{I-By} values. At the lower panel of the Figure (11, b), the frequency dependence of $R_{I-By} > 0.1$ $\mathrm{A^2/nT^2}$ probability $P_{0.1}$ is shown for the same two groups of pulsations, as at the 11a panel.

$P_{0.1}$ is 2 to 3 times higher for the large-scale than for small-scale pulsations, and at $f > 3$ mHz it exceeds 0.1, i.e. at these frequencies for each tenth interval the GIC to By PSD ratio exceeds 0.1 A^2/nT^2.

Discussion

Using the GIC and magnetic field data recorded in the Russian North and Fennoscandia in 2015, we have analyzed the influence of Pc5/Pi3 spatial scale on the efficiency of GIC generation. Our results are based on the analysis of GIC in the EPL prolongated along the meridian and B_Y component of geomagnetic pulsations.

The GIC to B_Y PSD spectral ratio R_{I-By} varies from 10^{-4} to 1 A^2/nT^2 with most probable values of $1 - 3 \cdot 10^{-2}$ A^2/nT^2 depending on pulsation frequency and spatial scale. The pulsation scale in the E-W direction (transversal to the EPL), is important, because the magnetic field of E-W short-scale pulsations can differ essentially at longitudes of the EPL and magnetic station.

The N-S large-scale pulsations generate more intensive GICs than the short-scale pulsations of the same amplitudes. Dependence of Pc5/Pi3 GIC efficiency on phase and coherence is stronger than on PSD distribution along a meridian.

A non-monotonous dependence of R_{I-By} on frequency, found for the $L_\gamma S_\varphi$ group (coherent pulsations with high phase difference), is probably associated with the FLR (Baransky et al, 1995). Although, this effect is expressed brightly in B_X, weaker resonance features are also found in meridional distribution of B_Y amplitude and phase (Lifshicz and Fedorov, 1986). In the vicinity of a resonance latitude, phase and amplitude gradients are higher than at non-resonant latitudes and the pulsation amplitude grows southward. In the case of a meridional EPL, R_{I-By} decreases with absolute value of phase difference. Meanwhile, for the system analyzed, R_{I-By} increases with the South-to-North PSD ratio. As a result, phase and amplitude gradients have opposite influence on the efficiency of GIC generation. The combination of these two factors can lead to a non-monotonous dependence of R_{I-By} on frequency.

The slopes of R_{I-By} spectra, shown in Figure 11, differ for the two groups of pulsations. For large- and small-scale pulsations it corresponds to $\alpha = 0.5$ and 1, respectively in the Eq.(1). Under the average conductivity in Fennoscandia of about 10^{-4} S/m, the skin depth for the $1.5 - 5$ mHz frequency band is about several hundred kilometers. For such values of conductivity, wavelength of large-scale pulsations exceeds the skin depth. In the case of small-scale pulsations, effective depth of the GIC electric circuit is of the same order of magnitude as the pulsation wavelength. This explains the difference in effective conductivity distributions between these two cases.

The statistical analysis of pulsation intervals recorded during the year 2015 has shown that the yearly mean values of R_{I-By} are about three times higher for the N-S large-scale (L_{NS}) pulsations, than for the small-scale (S_{NS}) ones. Meanwhile, a lower contrast in frequency integrated R_{I-By} values is obtained for the conductivity distributions described by the Eq. 1 with $\alpha = 0.5$ and 1. This means, that Pc3/Pi5 GIC efficiency depends on pulsation's scale at least as much as on conductivity distribution from the ground surface to the skin-depth.

Meanwhile, our present knowledge of magnetic field polarization, frequency and spatial distribution for different kinds of geomagnetic disturbances is not enough

for GIC applications. Actually, the absolute majority of publications is based on the data on extremal geomagnetic disturbances like magnetic storms. These disturbances are global. Therefore, the problem of spatial scale analysis does not exist for them.

The GICs generated at non-storm time are not so extensively studied. Amplitudes of non-storm GICs are lower than those of storm-time ones. However, background variations of moderate amplitudes may be even more important because they occur more often and it is more difficult to predict them.

In a general case, a theoretical solution for GIC can be obtained for a spatial harmonic and then integrated. An empirical model for spatial distribution of pulsation magnetic field would be necessary for that. Incomplete data on Earth conductivity distribution and on the elements of an electric network calls for a comprehensive empirical study of the GIC dependence on pulsation spectra, polarization and spatial distribution. However, at present, our understanding of ULF related GICs is limited even for Pc5 pulsations, whereas quasi-sinusoidal waves are not the only type of auroral disturbances. During severe disturbances, intensive irregular broadband variations are also common (see, e.g. (Posch et al, 2003)). GIC efficiency of some of these pulsations may be higher than that of the usual Pc5s. A similar effect can be caused by a coincidence of wave and bay-like disturbances (Yagova et al, 2018).

If wave field is essentially inhomogeneous, a qualitative technique employed in the present study, based on division into groups and accumulation of phase and amplitude information as separate parameters, may be of use. The above analysis allows to estimate the boundary between large- and small-scale pulsations as $2-5\cdot10^2$ km, depending on the direction and a particular variable studied. It is worth noting, that the meaning of the term "small-scale pulsation" can be different depending on the problem analyzed. A pulsation scale in the GIC problem is defined by phase and amplitude variation at an EPL length for the direction along the EPL and between the EPL and the nearest magnetic station for the transversal direction. Meanwhile, these pulsations are usually classified as medium-scale in the papers devoted to wave properties in the magnetosphere (see, e.g. Mager et al (2019)).

The above analysis of auroral observations can only partly be applied to the problem of ULF-related GICs at low and middle latitudes. Here, different effects are expected for Pc5 and Pc3-4 frequency ranges.

Pc5/Pi3 amplitudes at middle and low latitudes are high enough for GIC generation only during the main (Lee et al, 2007) or recovery (Kleimenova et al, 2005) phase of geomagnetic storms. These pulsations are usually global and almost in-phase at long distances along a meridian. However, essential amplitude and phase gradients are found near the plasmapause projection (Kale et al, 2007) and in the narrow near-equatorial region (Fedorov et al, 1999). This leads to non-negligible differences in the GICs modeled from magnetic measurements at different low-latitude sites (Ngwira et al, 2009). E-W distribution of Pc5 magnetic field at middle and low latitudes reproduces (in main features) its distribution at auroral latitudes. Thus, their E-W spatial scale can be important for GICs in EPLs prolongated in the E-W direction.

GICs generated by Pc3-4 pulsations have not been studied till now. Although, no extreme GIC amplitudes are expected for these pulsations, the question of potential

GIC risks related to these pulsations, is to be studied. This research is slowed by 1-minute time resolution typical for the majority of GIC measurements.

The new information about GIC dependence on pulsation properties is to be integrated into the existing picture of GIC generation. First, a consideration of interference of different inhomogeneities is necessary. The greatest effect can be expected for inhomogeneities of comparable spatial scales. Here, two separate topics maybe formulated: interference of wave finite wavelength effect with 1) inhomogeneity of the Earth conductivity and 2) configuration of the electric network. The first problem requires the inclusion of satellite data into analysis of ULF-related GICs to discriminate between space and ground sources of pulsation field gradients. For the second problem, finite pulsation wavelength should be included into the models of GIC dependence on electric network configuration (see e.g. Pirjola (2008) and references therein). Pirjola (2008) has proved that inter-node interaction becomes important at distances of about few dozen kilometers for spatially uniform magnetic field. In general, the role of distance between nodes was proved to be small. The low limit of pulsation spatial scale is about 100 km because of ionospheric screening (Kokubun et al, 1989). This value is high in comparison with the one, for which inter-node distance contributes to GIC. Thus, no essential synergetic effects between pulsation scale and inter-node distance are expected. Some inter-dependence of these two factors may occur only at auroral latitudes, where intensive pulsations with essential amplitude and phase gradients are common.

Conclusion

The pulsation spatial scale in frequency range of several milliHertz (Pc5/Pi3) influences their efficiency in GIC generation and similarity of geomagnetic and GIC pulsations. The statistical and case studies of GIC and geomagnetic pulsations were carried out with the geomagnetic and GIC data recorded in 2015 in the "Northern Transit" EPL, prolongated along the meridian. Higher coherence between geomagnetic and GIC variations is found for the E-W large-scale pulsations. The N-S large-scale pulsations generate more intensive GICs, than the small-scale pulsations of the same amplitudes. The spectral power of GICs generated by large-scale pulsations is three times higher, than for the small-scale ones. This proves, that at auroral latitudes, horizontal inhomogeneity of pulsation magnetic field is an important factor controlling their efficiency in GIC generation.

Availability of data and materials

Calculated spectra are available as supplementary files.

Competing interests

The authors declare that they have no competing interests.

Author's contributions

N.V. Yagova: data processing and interpretation of results; V.A. Pilipenko: interpretation of results, review and analysis of previous studies, theoretical estimates; Ya.A. Sakharov: GIC data preliminary analysis and selection of events; V.N. Selivanov: maintaining GIC observations, preliminary data processing; all the authors: preparation of the MS.

Funding

This work was supported by the Russian Science Foundation, Grant 16-17-00121.

Acknowledgements

We thank the institutes who maintain the IMAGE Magnetometer Array: TromsøGeophysical Observatory of UiT the Arctic University of Norway (Norway), Finnish Meteorological Institute (Finland), Institute of Geophysics Polish Academy of Sciences (Poland), GFZ German Research Centre for Geosciences (Germany), Geological Survey of Sweden (Sweden), Swedish Institute of Space Physics (Sweden), Sodankylä Geophysical Observatory of the University of Oulu (Finland), and Polar Geophysical Institute (Russia).

Abbreviations

- **CGM**: Corrected GeoMagnetic (coordinates)
- **EMF**: Electromotive force
- **EPL**: Electric Power Line
- **E-W**: East-West
- **FLR**: Field line Resonance
- **GIC**: Geomagnetically Induced Current
- **MHD**: Magneto-Hydro-Dynamic
- **MLT**: Magnetic local time
- **N-S**: North-South
- **Pi**: Pulsations Irregular
- **Pc**: Pulsations Continious
- **PDF**: Probability density function
- **PSD**: Power Spectral Density
- **ULF**: Ultra Low Frequency
- **UT**: Universal time

Author details

[1]Schmidt Institute of Physics of the Earth of the Russian Academy of Sciences (IPE RAS), B. Gruzinskaya 10, Moscow, Russia. [2]The Geophysical Center of the Russian Academy of Sciences (GC RAS), Molodezhnaya 3, Moscow, Russia. [3]Polar Geophysical Institute, Kola Science Center of the Russian Academy of Sciences, Akademgorodok, 26A, Apatity, Russia. [4]Northern Energetics Research Center, Kola Science Center of the Russian Academy of Sciences Akademgorodok, 21A, Apatity, Russia.

References

Alperovich LS, Fedorov EN (2007) In: Birton (ed) Hydromagnetic Waves in the Magnetosphere and the Ionosphere. Series: Astrophysics and Space Science Library, Springer, 426 pp, Netherlands

Apatenkov SV, Sergeev VA, Pirjola R, Viljanen A (2004) Evaluation of the geometry of ionospheric current systems related to rapid geomagnetic variations. Ann Geophys 22:63–72

Apatenkov SV, Pilipenko VA, Gordeev EI, Viljanen A, Juusola L, Belakhovsky VB, Sakharov YA, Selivanov VN (2020) Auroral omega bands are a significant cause of large geomagnetically induced currents. Geophys Res Lett 47(e2019GL086677)

Baddeley LJ, Yeoman TK, Wright DM, Trattner KJ, Kellet BJ (2004) A statistical study of unstable particle populations in the global ringcurrent and their relation to the generation of high m ulf waves. Ann Geophys 22:4229–4241

Baker G, Donovan EF, Jackel BJ (2003) A comprehensive survey of auroral latitude pc5 pulsation characteristics. J Geophys Res: Space Phys 108(1384)

Baransky LN, Fedorov EN, Kurneva NA, Pilipenko VA, Green AW, Worthington EW (1995) Gradient and polarization methods of the ground-based hydromagnetic monitoring of magnetospheric plasma. J Geomagn Geolect 47:1293–1309

Bedrosian PA, Love JJ (2015) Mapping geoelectric fields during magnetic storms: Synthetic analysis of empirical united states impedances. Geophys Res Lett 42:10,160–10,170

Belakhovsky V, Pilipenko V, Sakharov Y, Selivanov V (2018) Characteristics of the variability of a geomagnetic field for studying the impact of the magnetic storms and substorms on electrical energy systems. Izvestiya, Physics of the Solid Earth 54(1):52–65

Belakhovsky V, Pilipenko V, Engebretson M, Sakharov Y, Selivanov V (2019) Impulsive disturbances of the geomagnetic field as a cause of induced currents of electric power lines. Journ Space Weath Space Clim 9(A18)

Boteler DH (2001) Space weather effects on power systems. In: Song SHJ P, Siscoe G (eds) Space Weather, AGU, Washington, pp 347–352

Boteler DH, Pirjola RJ (2017) Modeling geomagnetically induced currents. Space Weather 15:258– 276

Chisham G, Mann IR (1999) A Pc5 ULF wave with large azimuthal wavenumber observed within the morning sector plasmasphere by sub-auroral magnetometer network. J Geophys Res: Space Phys 104:14,717–14,727

Engebretson MJ, Steinmetz ES, Posch JL, Pilipenko VA, Moldwin MB, Connors MG, Boteler DH, Mann IR, Hartinger MD, Weygand JM, Lyons LR, Nishimura Y, Singer HJ, Ohtani S, Russell CT, Fazakerley SA, Kistler SA (2019) Nighttime magnetic perturbation events observed in Arctic Canada: 2. multiple-instrument observations. J Geophys Res: Space Phys 124:7459–7476

Fedorov E, Pilipenko V, Surkov V, Rao DRK, Yumoto K (1999) Ionospheric propagation of magnetohydrodynamic disturbances from the equatorial electrojet. J Geophys Res: Space Phys 104:4329–4336

James MK, Yeoman TK, Mager PN, Klimushkin DY (2013) The spatio-temporal characteristics of ULF waves driven by substorm injected particles. J Geophys Res: Space Phys 118:1737–1749

Kale ZC, Mann IR, Waters CL, Goldstein J, Menk FW, Ozeke LG (2007) Ground magnetometer observation of a cross-phase reversal at a steep plasmapause. J Geophys Res: Space Phys 112(A10222)

Kappenman J (2004) The evolving vulnerability of electric power grids. Space Weather 2(S01004)

Kay SM (1988) In: Modern spectral estimation: Theory and application, Prentice-Hall, New Jersey, USA, p 543 pp.

Kleimenova NG, Kozyreva OV, Manninen J, Ranta A (2005) Unusual strong quasi-monochromatic ground Pc5 geomagnetic pulsations in the recovery phase of November 2003 superstorm. Ann Geophys 23:2621–2634
Kokubun S, Erickson KN, Fritz TA, McPherron RL (1989) Glocal time asymmetry of Pc 4-5 pulsations and associated particle modulations at synchronous orbit. J Geophys Res: Space Phys 94:6607–6625
Lee EA, Mann IR, Lotoaniu T, Dent ZC (2007) Global Pc5 pulsations observed at unusually low l during the great magnetic storm of 24 March 1991. J Geophys Res: Space Phys 112(A05208)
Lifshicz AE, Fedorov EN (1986) Hydromagnetic oscillations of the magnetosphere-ionosphere resonator. Docl USSR Acad Sci 287:90–95
Love JJ, Lucas GM, Kelbert A, Bedrosian PA (2018) Geomagnetically induced currents modeling and forecasting. Space Weather 16:1114–1127
Lucas GM, Love JJ, Kelbert A, Bedrosian PA, Rigler EJ (2020) A 100-year geoelectric hazard analysis for the U.S. high-voltage power grid. Space Weather 18(e2019SW002329)
Mager OV, Chelpanov MA, Mager PN, Klimushkin DY (2019) Conjugate ionosphere-magnetosphere observations of a sub-alfvenic compressional intermediate-m wave: A case study using EKB radar and Van Allen probes. Journ Geophys Res: Space Phys 124:3276–3290
Mager PN, Klimushkin DY, Kostarev DV (2013) Drift-compressional modes generated by inverted plasma distributions in the magnetosphere. Journ Geophys Res: Space Phys 118:4915–4923
Marin J, Pilipenko V, Kozyreva O, Stepanova M, Engebretson M, Vega P, Zesta E (2014) Global Pc5 pulsations during strong magnetic storms: excitation mechanisms and equatorward expansion. Annales Geophysicae 32:319–331
Mazur VA, Chuiko DA (2017) Energy flux in 2-D MHD waveguide in the outer magnetosphere. Journ Geophys Res: Space Phys 122:1946–1959
Menk FW, Mann IR, Smith AJ, Waters CL, Clilverd MA, Milling DK (2004) Monitoring the plasmapause using geomagnetic field line resonances. Journ Geophys Res: Space Phys 109(A04216)
Milling DK, Mann IR, Menk FW (2001) Diagnosing the plasmapause with a network of closely spaced ground?based magnetometers. Geophys Res Lett 28:115–118
Ngwira CM, McKinnell LA, Cilliers PJ, Viljanen A, Pirjola R (2009) Limitations of the modeling of geomagnetically induced currents in the South African power network. Space Weather 7(S10002)
Pilipenko V, Yumoto K, Fedorov E, Yagova N (1999) Hydromagnetic spectroscopy of the magnetosphere with Pc3 geomagnetic pulsations along the 210 meridian. Ann Geophys 17:53–65
Pirjola R (2008) Effects of interactions between stations on the calculation of geomagnetically induced currents in an electric power transmission system. Earth Planet Sp 60:743–751
Posch JL, Engebretson MJ, Pilipenko VA, Hughes WJ, Russell CT, Lanzerotti LJ (2003) Characterizing the long-period ULF response to magnetic storms. Journ Geophys Res: Space Phys 108(1029)
Pulkkinen A (2015) Geomagnetically induced currents modeling and forecasting. Space Weather 13:734–736
Pulkkinen A, Kataoka R (2006) S-transform view of geomagnetically induced currents during geomagnetic superstorms. Geophys Res Lett 33(L12108)
Pulkkinen A, Hesse M, Kuznetsova M, Rastssatter L (2007) First-principles modeling of geomagnetically induced electromagnetic fields and currents from upstream solar wind to the surface of the Earth. Ann Geophys 25:881–893
Sakharov YA, Yagova NV, Pilipenko VA (2021) Pc5/Pi3 geomagnetic pulsations and geomagnetically induced currents. Bull. Russian Acad. Sci.: Physics 85 (In press)
Sandhu JK, Yeoman TK, James MK, Rae IJ, Fear RC (2018) Variations of high-latitude geomagnetic pulsation frequencies: A comparison of time-of-flight estimates and IMAGE magnetometer observations. Journ Geophys Res: Space Phys 123:567– 586
Tanskanen EI (2009) A comprehensive high-throughput analysis of substorms observed by image magnetometer network: Years 1993-2003 examined. J Geophys Res 114(A05204)
Viljanen A (1998) Relation of geomagnetically induced currents and local geomagnetic field variations. Trans Power Deliv 13:1285–1290
Viljanen A, Nevanlinna H, Pajunpaa K, Pulkkinen A (2001) Time derivative of the horizontal geomagnetic field as an activity indicator. Ann Geophys 19(A17)
Viljanen A, Pulkkinen A, Amm O, Pirjola R, Korja T, Group BW (2004) Fast computation of the geoelectric field using the method of elementary current systems and planar earth models. Ann Geophys 22:101–113
Viljanen A, Pirjola R, Wik M, Adam A, Pracser E, Sakharov Y, Katkalov J (2012) Continental scale modelling of geomagnetically induced currents. J Space Weather Space Clim 2,
Yagova NV, Heilig B, Fedorov EN (2015) Pc2-3 geomagnetic pulsations on the ground, in the ionosphere, and in the magnetosphere: MM100, CHAMP, and THEMIS observations. Ann Geophys 33:117–128
Yagova NV, Pilipenko VA, Fedorov EN, Lhamdondog AD, Gusev YP (2018) Geomagnetically induced currents and space weather: Pi3 pulsations and extreme values of time derivatives of the geomagnetic field's horizontal components. Izvestiya, Physics of the Solid Earth 54:749–763

Figures

Figure 1 Locations of the magnetic observatories, the observational point of GIC recording at VKH. The electric power line is schematically shown with a red dashed line

Tables

Figure 2 Event 1 Pulsations recorded in the geomagnetic field and GIC on day 2015 060. (a) waveforms of B_Y pulsations at KEV (magenta) and GIC at VKH (dark blue); (b) normalized PSD spectra; (c) $B-I$ spectral coherence for B_Y (solid line) and B_X - (dashed); (d) GIC to B_Y PSD ratio

Figure 3 Parameters of the event 1 pulsation in the E-W direction: (a) B_Y waveforms at KEV (magenta) and KIL (green); (b) normalized PSD spectra; (c) E-W spectral coherence for B_Y (solid) and B_X (dashed); (d) E-W PSD ratio for B_Y (solid), and B_X (dashed)

Figure 4 Parameters of the event 1 pulsation in the N-S direction: (a) and (b) B_Y and B_X waveforms at KEV (magenta) and SOD (blue); (c) normalized PSD spectra; (d) and (e) N-S spectral coherence and phase difference for B_Y (solid) and B_X - (dashed); (f) South-to-North PSD ratio for B_Y (solid) and B_X - (dashed)

Figure 5 Event 2 Pulsations recorded in the geomagnetic field and GIC on day 2015 132. (a) waveforms of B_Y pulsations at KEV (magenta) and GIC at VKH (dark blue); (b) normalized PSD spectra; (c) $B-I$ spectral coherence for B_Y (solid) and B_X (dashed); (d) I to B_Y PSD ratio

Figure 6 Parameters of the event 2 pulsation in the E-W direction: (a) B_Y waveforms at KEV (magenta) and KIL (green); (b) normalized PSD spectra; (c) E-W spectral coherence for B_Y (solid) and B_X (dashed); (d) E-W PSD ratio for B_Y (solid) and B_X (dashed)

Figure 7 Parameters of the event 2 pulsation in the N-S direction: (a) and (b) B_Y and B_X waveforms at KEV (magenta) and SOD (blue); (c) normalized PSD spectra; (d) and (e) N-S spectral coherence and phase difference for B_Y (solid) and B_X - (dashed); (f) South-to-North PSD ratio for B_Y (solid) and B_X - (dashed)

Figure 8 γ^2_{I-By} empirical PDF for the E-W large- (L_{EW}) and small-scale (S_{EW}) pulsations

Figure 9 R_{I-By} normalized PDF for the N-S large (L_{NS}) small-scale (S_{NS}) pulsations

Figure 10 Averaged R_{I-By} spectra for 6 groups of pulsations: 1)-2) small-scale S_γ and large-scale L_γ in accordance to the N-S spectral coherence; 3)-4) $L_\gamma S_\varphi$ and $L_\gamma L_\varphi$ are the small-/large-scale sub-groups of the L_γ group defined in accordance to the phase difference; 5)-6) $L_\gamma L_\varphi S_P$ and $L_\gamma L_\varphi L_P$ are the small- /large-scale sub-groups of the $L_\gamma L_\varphi$ groups defined in accordance to the South-to-North PSD ratio.

Figure 11 (a) Averaged R_{I-By} spectra for the N-S large- (L_{NS}) and small-scale (S_{NS}) pulsations. ($L_{NS} = L_\gamma L_\varphi L_P$ in Figure 10, while all the other groups form the S_{NS} group) ; (b) frequency dependence of $R_{I-By} > 0.1$ $\mathrm{A^2/nT^2}$ fraction for the same groups of pulsations

Table 1 Stations Information

Station	Code	Geographic		CGM		UT of MLT
		LAT	LON	LAT(Φ)	LON(Λ)	midnight
Kevo	KEV	69.76	27.01	66.65	108.35	21:06
Kilpisjärvi	KIL	69.02	20.79	66.13	102.80	21:28
Sodankylä	SOD	67.37	26.63	64.22	106.52	21:13
Vykhodnoy	VKH	68.83	33.08	65.53	112.73	20:49

Figures

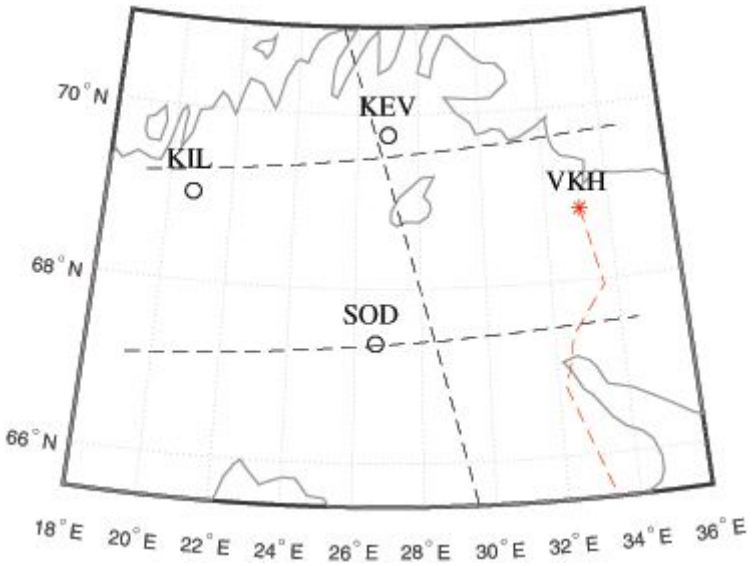

Figure 1

Locations of the magnetic observatories, the observational point of GIC recording at VKH. The electric power line is schematically shown with a red dashed line

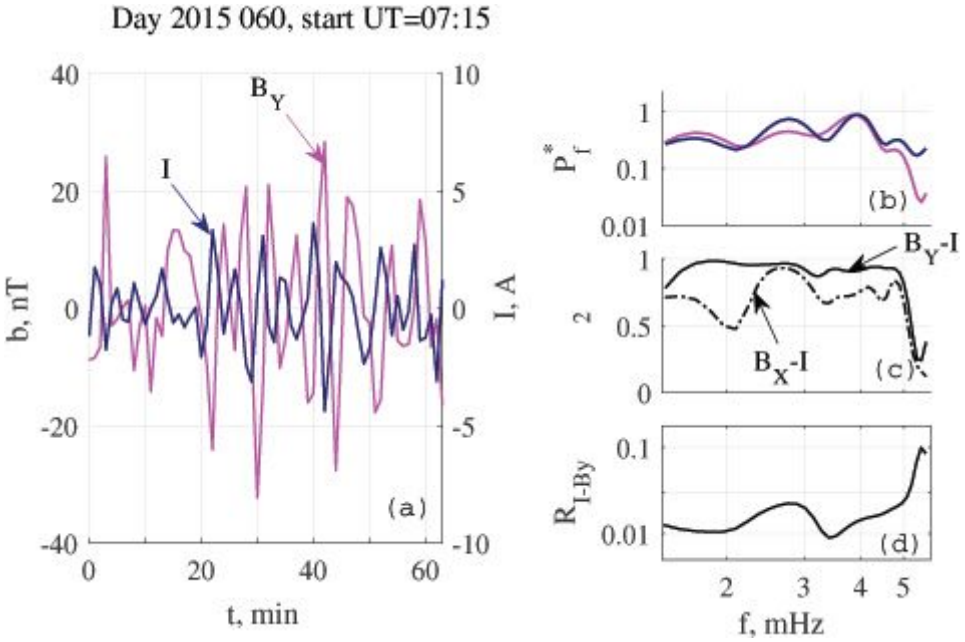

Figure 2

Event 1 Pulsations recorded in the geomagnetic field and GIC on day 2015 060. (a) waveforms of BY pulsations at KEV (magenta) and GIC at VKH (dark blue); (b) normalized PSD spectra; (c) B – I spectral coherence for BY (solid line) and BX - (dashed); (d) GIC to BY PSD ratio

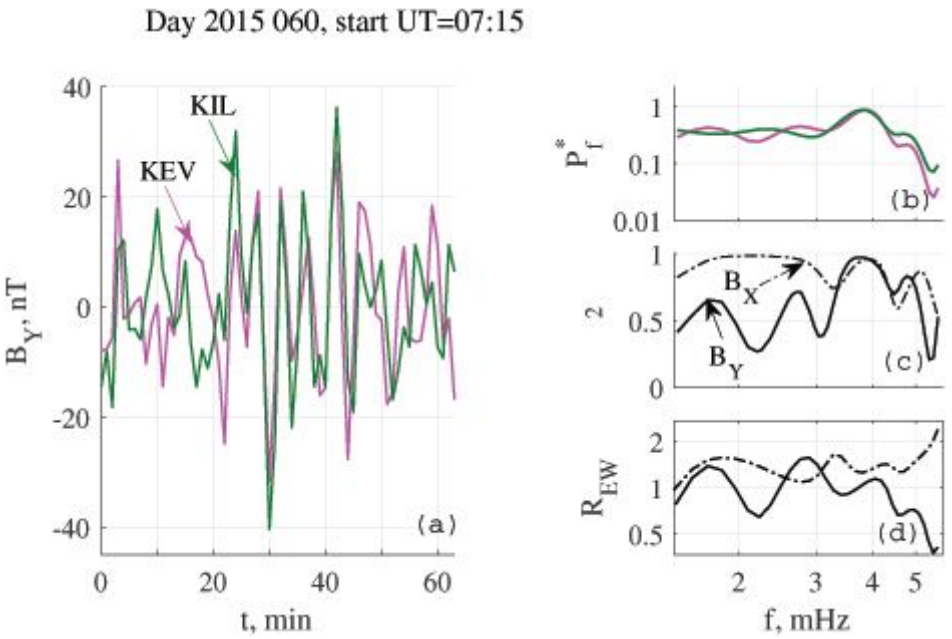

Figure 3

Parameters of the event 1 pulsation in the E-W direction: (a) BY waveforms at KEV (magenta) and KIL (green); (b) normalized PSD spectra; (c) E-W spectral coherence for BY (solid) and BX (dashed); (d) E-W PSD ratio for BY (solid), and BX (dashed)

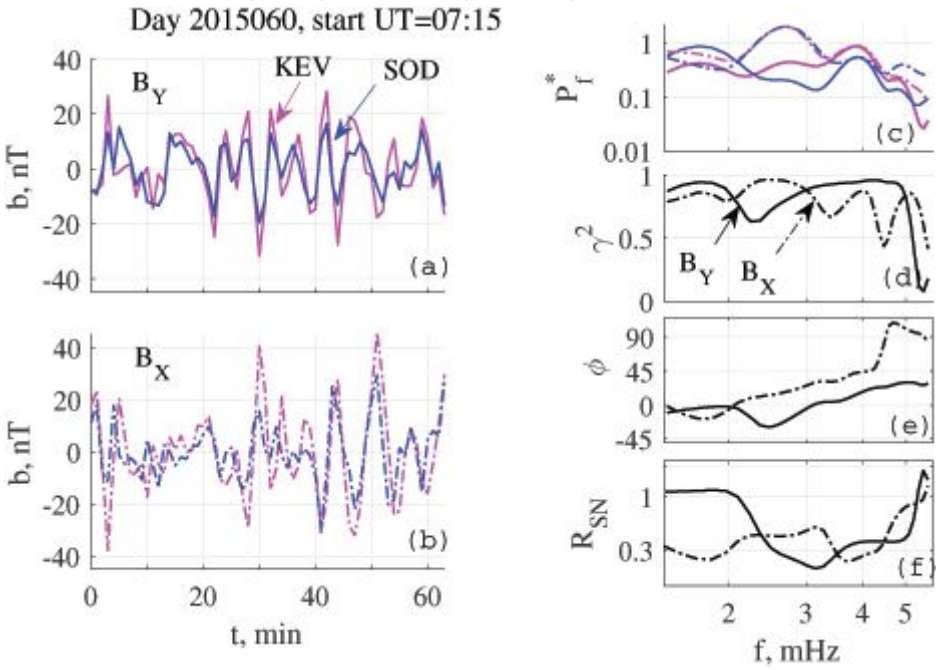

Figure 4

Parameters of the event 1 pulsation in the N-S direction: (a) and (b) BY and BX waveforms at KEV (magenta) and SOD (blue); (c) normalized PSD spectra; (d) and (e) N-S spectral coherence and phase difference for BY (solid) and BX - (dashed); (f) South-to-North PSD ratio for BY (solid) and BX - (dashed)

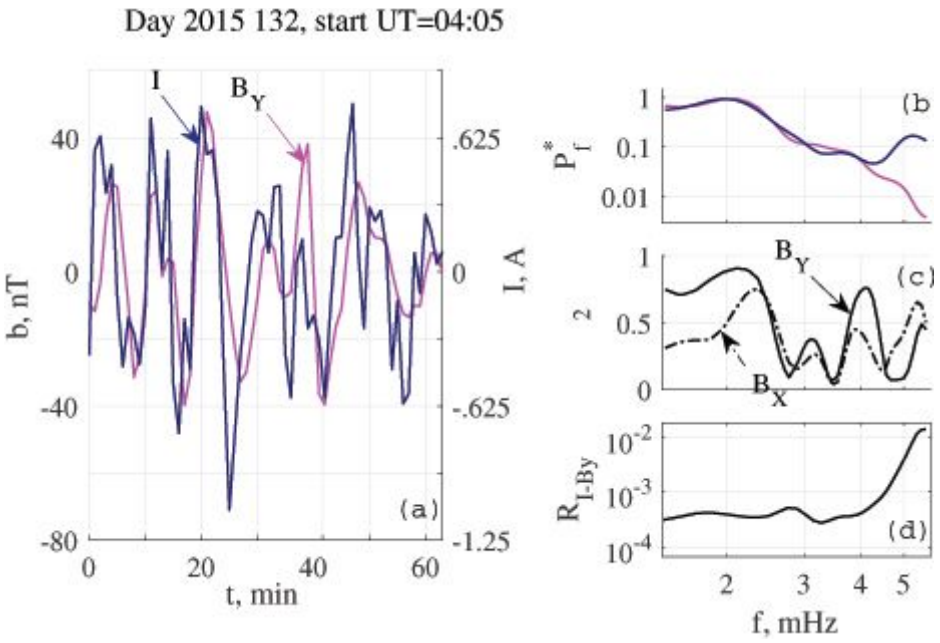

Figure 5

Event 2 Pulsations recorded in the geomagnetic field and GIC on day 2015 132. (a) waveforms of BY pulsations at KEV (magenta) and GIC at VKH (dark blue); (b) normalized PSD spectra; (c) B − I spectral coherence for BY (solid) and BX (dashed); (d) I to BY PSD ratio

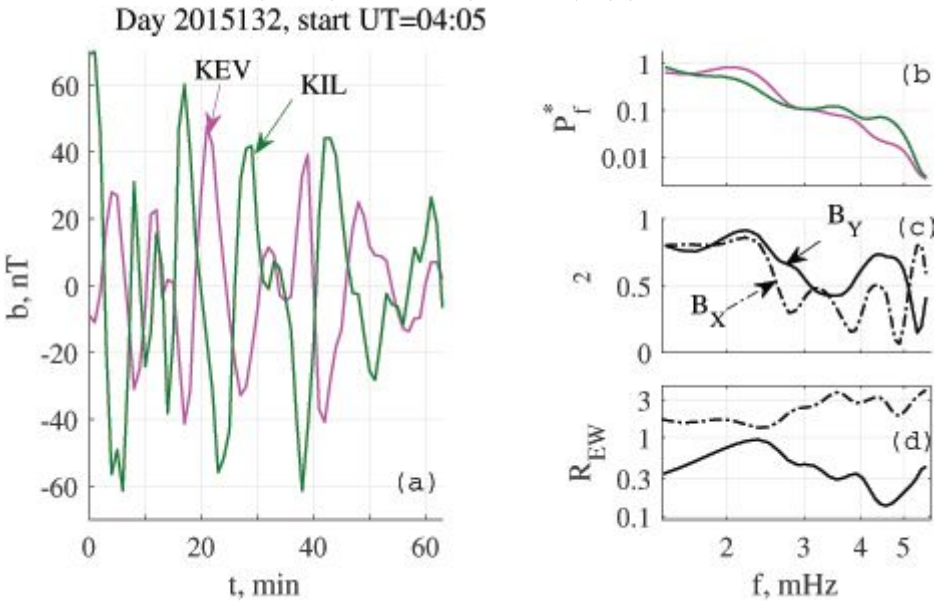

Figure 6

Parameters of the event 2 pulsation in the E-W direction: (a) BY waveforms at KEV (magenta) and KIL (green); (b) normalized PSD spectra; (c) E-W spectral coherence for BY (solid) and BX (dashed); (d) E-W PSD ratio for BY (solid) and BX (dashed)

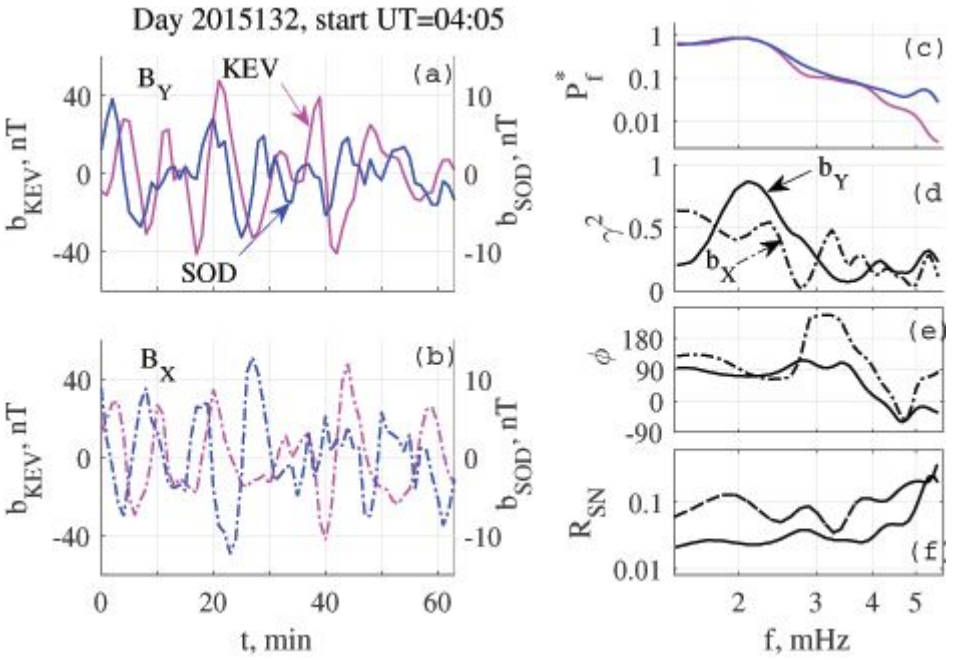

Figure 7

Parameters of the event 2 pulsation in the N-S direction: (a) and (b) BY and BX waveforms at KEV (magenta) and SOD (blue); (c) normalized PSD spectra; (d) and (e) N-S spectral coherence and phase difference for BY (solid) and BX - (dashed); (f) South-to-North PSD ratio for BY (solid) and BX - (dashed)

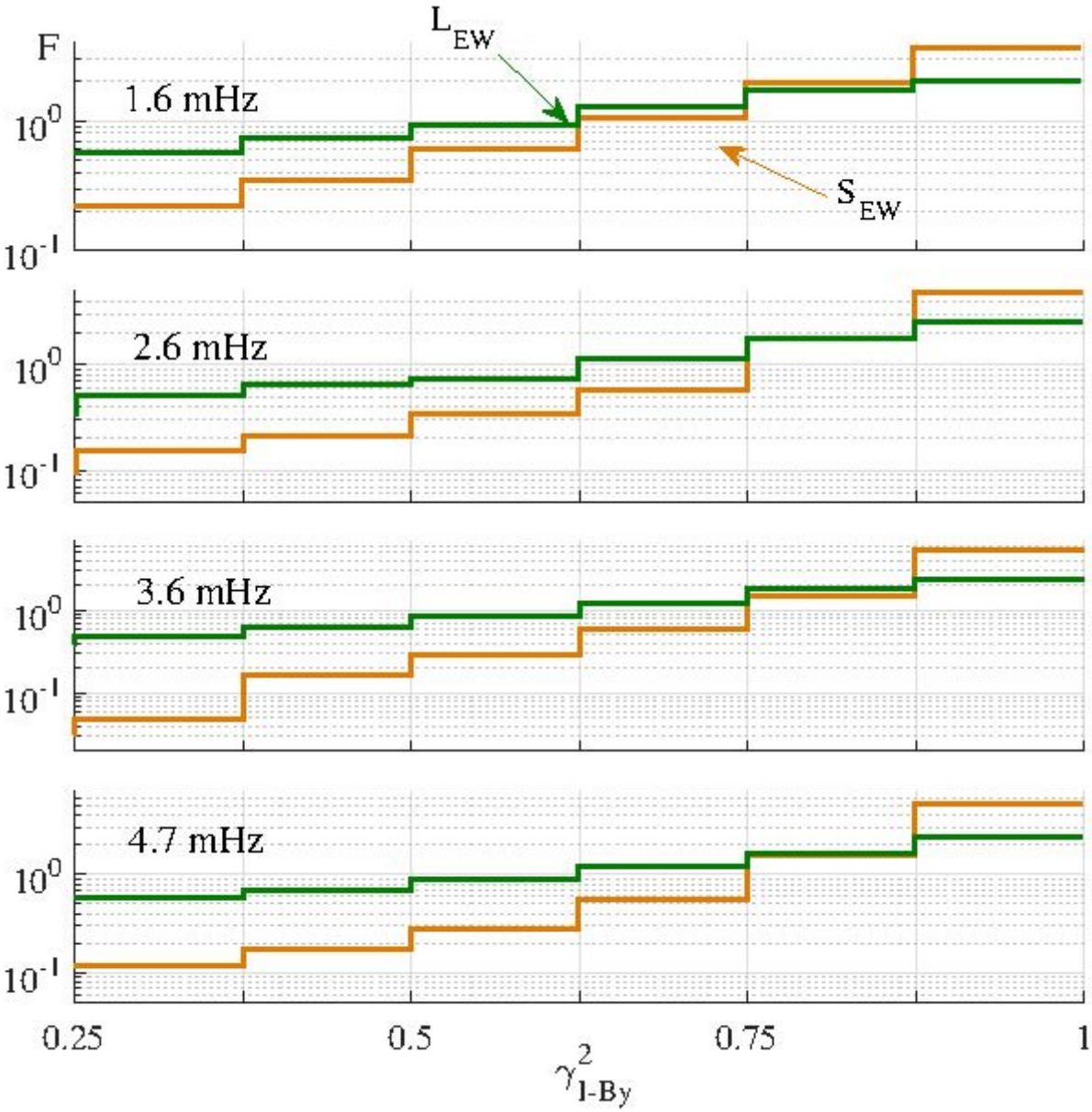

Figure 8

γ2 I−By empirical PDF for the E-W large- (LEW) and small-scale (SEW) pulsation

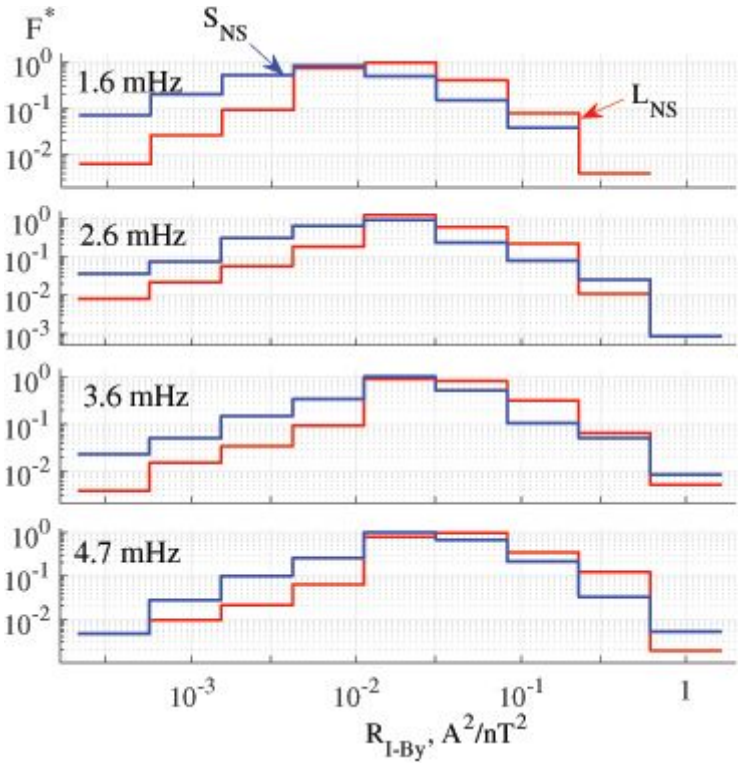

Figure 9

RI−By normalized PDF for the N-S large (LNS) small-scale (SNS) pulsations

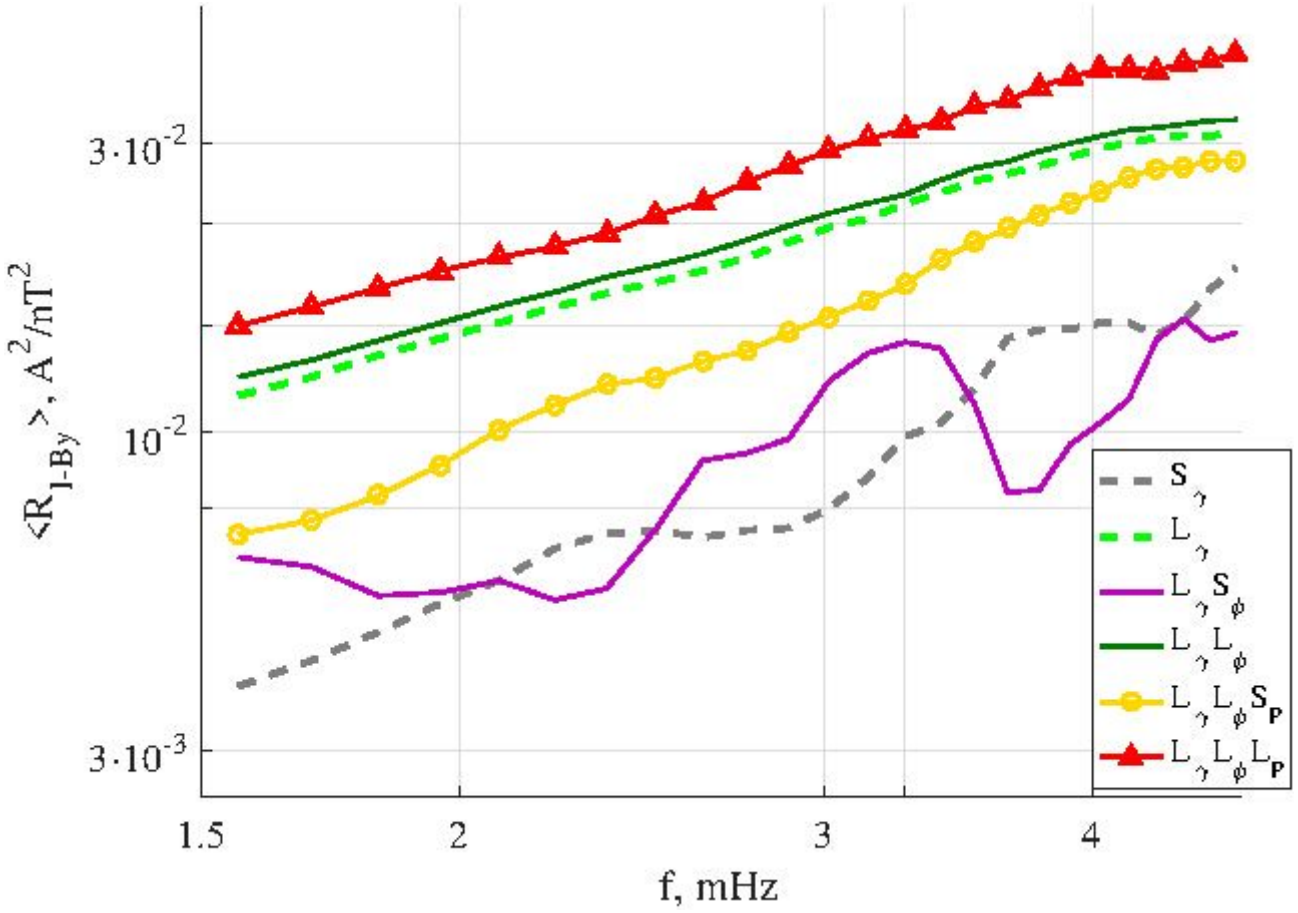

Figure 10

Averaged RI−By spectra for 6 groups of pulsations: 1)-2) small-scale Sγ and large-scale Lγ in accordance to the N-S spectral coherence; 3)-4) LγS□ and LγL□ are the small-/large-scale sub-groups of the Lγ group defined in accordance to the phase difference; 5)-6) LγL□SP and LγL□LP are the small- /large-scale sub-groups of the LγL□ groups defined in accordance to the South-to-North PSD ratio.

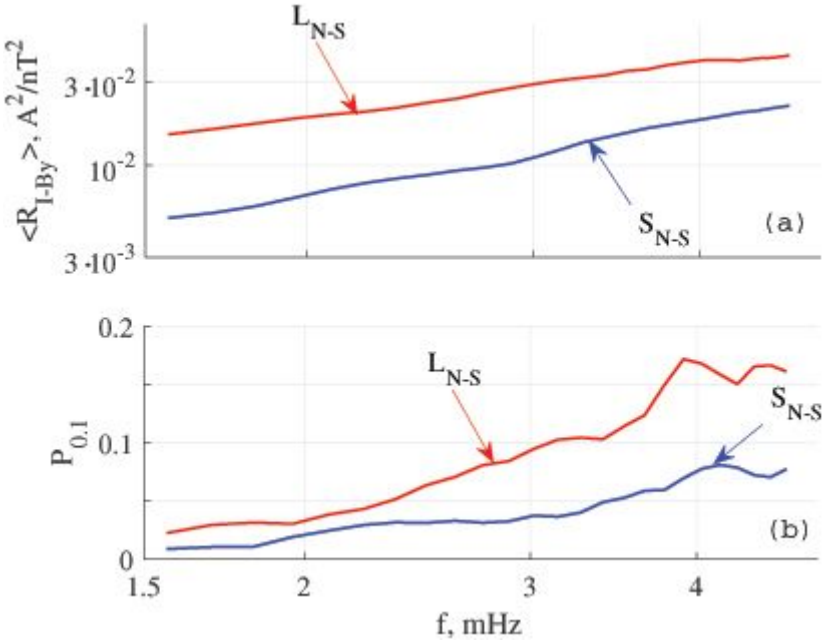

Figure 11

(a) Averaged RI−By spectra for the N-S large- (LNS) and small-scale (SNS) pulsations. (LNS = LγL□LP in Figure 10, while all the other groups form the SNS group) ; (b) frequency dependence of RI−By > 0.1 A2/nT2 fraction for the same groups of pulsations

Supplementary Files

This is a list of supplementary files associated with this preprint. Click to download.

- YagovaPc5GIcgrabst.pdf